Tracer Leakage from Modeled Agulhas Rings

L. DE STEUR AND P. J. VAN LEEUWEN

Institute for Marine and Atmospheric Research at Utrecht, Utrecht, Netherlands

S. S. DRIJFHOUT

Royal Netherlands Meteorological Institute (KNMI), De Bilt, Netherlands

(Manuscript received 7 November 2002, in final form 2 January 2004)

ABSTRACT

In a numerical, isopycnal, ocean model the mixing is investigated with the environment of two idealized Agulhas rings, one that splits, and one that remains coherent. The evolution of a passive tracer, initially contained within the rings, shows that tracer leakage is associated with the formation of filaments in the early stage of ring evolution. These filaments reach down to the thermocline. In the deepest layers leakage occurs on a larger scale. Self-advection of the rings is very irregular, and it is not possible to compute a Lagrangian boundary in order to estimate the transport of leakage from the rings. To describe the processes that govern tracer leakage, in a coordinate frame moving with the ring a kinematic separatrix is defined in the streamfunction field for the nondivergent flow. Initially, filaments arise because of the elongation of the ring, which is mainly governed by an $m = 2$ instability that is collaborating with differential rotation. Because of beta, the symmetry is destroyed related to the separatrix associated with a stagnation point in the flow. The filament upstream of the stagnation point grows much faster and is associated with the bulk of tracer leakage. Mixing is enhanced by time dependence of the separatrix. As a result, there are no large differences between the leakage from a coherent ring, where the $m = 2$ instability equilibrates, and from a splitting ring, where the $m = 2$ instability keeps growing, which confirms that the amount of leakage is mainly governed by the ring's initial deformation combined with unsteady self-advection of the ring and not by the splitting of the ring. The decay of tracer content in the thermocline shows that in the first months up to 40% of the ring water can be mixed with the environment. In deeper layers the decay of tracer content may reach up to 90%.

1. Introduction

Oceanic rings are important in distributing properties like heat and salt through the world's oceans. Agulhas rings are thought to play a key role in the Indian–Atlantic interocean exchange and in maintaining the global overturning circulation through the so-called warm-water route (Gordon 1986; De Ruijter et al. 1999; Weijer et al. 1999). After Agulhas rings are shed from the Agulhas Current, they move into the highly variable Cape Basin where they interact with bottom topography and other rings (Byrne et al. 1995; Schouten et al. 2000). The number of Agulhas ring-shedding events ranges on average from 4 to 6 times per year (Feron et al. 1992; Goñi et al. 1997; Duncombe Rae et al. 1996). As the rings move into the southeastern Atlantic Ocean their SSH anomaly decays remarkably, as has been observed using satellite altimetry (Byrne et al. 1995; Schouten et al. 2000). On average one-half of the SSH decay takes place during the first 5 months of their lifetime; see Fig. 1.

In 1999 the Mixing of Agulhas Rings Experiment (MARE) program was initiated, which consists of a large observational component and an extensive modeling program. The main goal of MARE is to estimate the proportion of Agulhas leakage that contributes to the upper branch of the global overturning circulation and to identify the dominant mixing processes that determine that proportion. The focus of the observational program was to determine the decay of Agulhas Ring Astrid, which was monitored three times at time intervals of 6 months. The measurements of the first cruise have been thoroughly described in Van Aken et al. (2003). In a model study the evolution of Agulhas rings and their SSH decay was investigated for a whole range of ring parameters (Drijfhout et al. 2003) and the observed SSH decay was very well reproduced. It was shown that strong rings are unstable and split into two or more parts. This has been supported by a linear stability analysis in which it was shown that equivalent barotropic rings are linearly unstable for an $m = 2$ mode that contributes to adjustment and splitting (Katsman et

Corresponding author address: L. de Steur, Princetonplein 5, 3584 CC, Utrecht, Netherlands.
E-mail: steur@phys.uu.nl

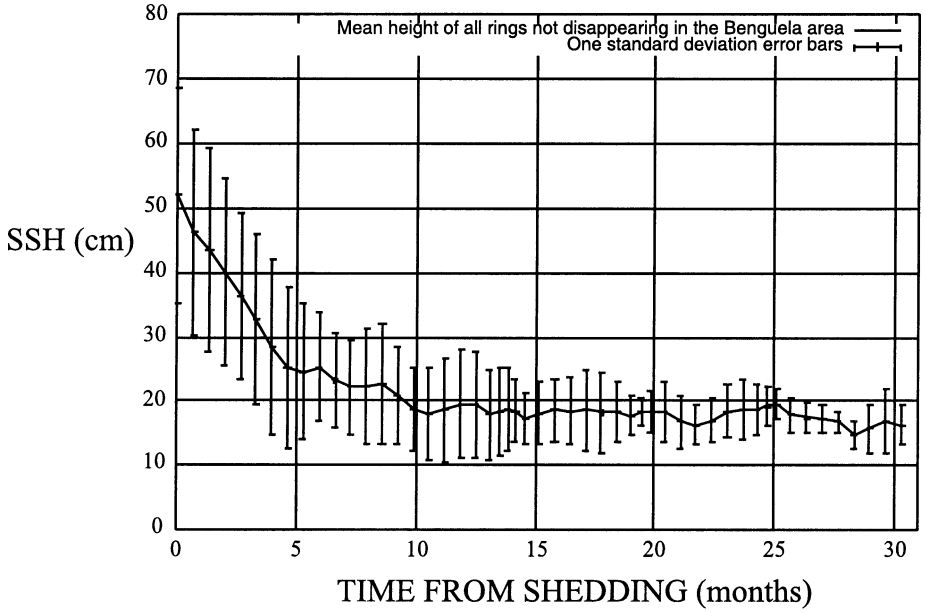

FIG. 1. Decay of Agulhas rings, after Schouten et al. (2000).

al. 2003). The modeled SSH decay in the early phase of ring evolution seemed to be associated with a mixed barotropic/baroclinic instability. The numerical simulation of Ring Astrid showed that tracer loss from the ring scaled well with SSH decay in the early phase of the ring evolution. The final splitting process did not seem to affect the SSH decay. This implies that the SSH decay is associated with mixing of thermodynamic properties of the ring with its surroundings. However, the mechanism that is responsible for this mixing had not been identified and an estimate of the magnitude of the mixing is still missing. Also it was not clear whether the similarity between SSH decay and tracer leakage can be generalized to other rings.

The numerical simulations of Agulhas rings showed formation of filaments and small-scale structures during its time evolution (Drijfhout et al. 2003). The formation of the filaments, which were finally shed from the ring, could be a possible, efficient mechanism for mixing of ring water. Filaments have been observed in the ocean, usually in the presence of ring structures, or at the edge of western boundary currents (Lutjeharms and Cooper 1996; Joyce et al. 1992). In Dewer and Flierl (1985), the impact of mixing of water from warm core Gulf Stream rings on the slope water was investigated with simple kinematic models. By comparing tracer distributions computed by a dynamic ring model with purely kinematic ring representations, cross-boundary transport and mixing could be described qualitatively. However, the exact amount of tracer leaking from Gulf Stream rings was not quantified.

Monopolar vortex filaments were investigated in both laboratory experiments (Kloosterziel and van Heijst 1992; Flór and van Heijst 1996) and numerical simulations (Legras and Dritschel 1993). In rotating tank experiments lobe shedding or filamentation from propagating vortices was observed (Carnevale and Kloosterziel 1994). Lobe shedding takes place when fluid inside the vortex crosses a so-called separatrix. The separatrix divides a region where the fluid is advected with the vortex from a region where the fluid remains behind. The fluid that is not trapped within the separatrix is then able to mix with the surrounding water. Mixing and transport have been thoroughly studied within the framework of dynamical systems theory where regions of different flow characteristics are separated by stable and unstable manifolds of the hyperbolic solution in a two-dimensional, incompressible flow (Pierrehumbert 1991; Rom-Kedar and Wiggins 1990; Wiggins 1992). These methods have been extended and applied successfully to quasiperiodic flow fields (Duan and Wiggins 1996; Miller et al. 1997; Rogersen et al. 1999) and to velocity fields with a slowly varying time dependence (Haller and Poje 1998; Poje and Haller 1999).

Here we make an effort to quantify ring decay of Agulhas rings due to filamentation using a primitive equation numerical model. The focus will be on the mixing of ring water associated with the fast decay during the first few months using two different rings: one that is quickly deforming by a mixed baroclinic/barotropic instability and finally splits and one that remains coherent and slowly deforms. In section 2 the model setup and initial ring profiles are given. The evolution of the rings, specifically of tracer released in the rings, is analyzed in section 3. Also, a method to quantify tracer leakage using a simple kinematic approach is given in here. In section 4 estimates of tracer leakage from the rings are given using three different ring boundaries,

and it is shown that the three ways of estimating the transport provide corresponding results. A discussion and the conclusions are given in section 5.

2. Model setup

The model used for the experiments is the Miami Isopycnic Coordinate Ocean Model (MICOM 2.7; Bleck and Smith 1990). We use a 1000 km × 1000 km double periodic domain with a horizontal resolution of 5 km and a flat bottom at 4000-m depth. In the vertical direction there are 12 isopycnal layers. Lateral diffusion and friction are biharmonic, bottom stress is parameterized by a quadratic drag relation. Diapycnal diffusion is set to zero. There is no wind or buoyancy forcing applied and the time evolution is completely determined by interior dynamics. On the time scales considered the viscous dissipation is negligible.

The initial rings are circular symmetric and equivalent barotropic. The 12 layers have been chosen such that the stratification mimics Ring Astrid as measured during the MARE-1 cruise (Van Aken et al. 2003). The undisturbed layer depths h_k^0 (where k is the layer index) are at 50, 100, 200, 300, 400, 500, 600, 700, 1000, 1600, 2500, and 4000 m. The amplitudes $h_k^{\max}$ of the model rings have been determined from the observations as follows: the σ_0 value at 50 m outside Ring Astrid is determined and the depth of this σ_0 value is assessed as a function of the radial distance from the ring center. The obtained depths of the observed Ring Astrid do not fit very well to a Gaussian profile, which is usually used in ring studies, but they fit best to a solid body profile matched to an exponential profile at $r = R$. This profile is given by

$$h_k(r) = h_k^0 + h_k^{\max}\left[1 - \frac{1}{2}\left(\frac{r}{R}\right)^2\right] \qquad \text{for } r < R \quad (1)$$

and

$$h_k(r) = h_k^0 + h_k^{\max}\frac{1}{2}\exp\left\{\frac{1}{2}\left[1 - \left(\frac{r}{R}\right)^4\right]\right\} \quad \text{for } r < R. \quad (2)$$

The same profile is used for all layer depths. The temperature profile is obtained in a similar way and salinity is calculated from the temperature and associated σ_0 values. The velocity field of the rings is initialized in cyclogeostrophic balance. The measurements have shown that the ring extends all the way to the bottom. To account for this, we assume a barotropic pressure gradient that overcompensates the baroclinic pressure gradient at the bottom, such that the rings are corotating.

In Drijfhout et al. (2003), the full-size Ring Astrid was simulated. The sensitivity of the ring evolution was investigated for different radii since Ring Astrid is an atypically large Agulhas ring. It was shown that most rings split up into many smaller ones for various values of R because of the growth of the $m = 2$ instability. Since the focus of this paper is on the process of mixing of a ring with its surroundings, we refrain from studying Ring Astrid, but chose two smaller rings for this purpose that show a more typical ring evolution. For the first ring, to be called ring A in the remaining sections, the $m = 2$ mode causes the ring to split into two halves after 80 days. For the second, smaller ring, called ring B, the $m = 2$ instability equilibrates after about 40 days and the ring remains coherent. The radius R is 97 km for ring A and 80 km for ring B, which corresponds with radii of maximum velocity at $L = 90$ km and at $L = 75$, respectively. The maximum velocity is 88 cm s^{-1} in the upper layer and 3 cm s^{-1} in the lowest layer for ring A. For ring B these velocities are 140 and 20 cm s^{-1}, respectively. The barotropic pressure in ring B is larger than in ring A, resulting in maximum barotropic velocities of 13 cm s^{-1} for ring A and 40 cm s^{-1} for ring B.

To analyze the mixing of ring water with its surroundings, passive tracer has been added to the rings within a defined boundary at $t = 0$. The initial boundary for initializing tracer has been chosen as a specific pressure level, defined for each layer as $B_k = p_k^0 + 5\%p_k^{\max}$. The passive tracer concentration was initialized as 1 inside and 0 outside the ring boundary B_k. In the following section the evolution of tracer relative to this boundary is discussed and it is shown how tracer leaks from the rings.

3. Evolution of tracer and processes governing filamentation

A detailed model study on the decay of Agulhas Ring Astrid (Drijfhout et al. 2003) showed that the modeled SSH decay agrees very well with the observations from altimetry measurements (Schouten et al. 2000). The robustness of this decay was investigated for a whole set of ring parameters. The model results suggested that the mixed barotropic/baroclinic instability accounts for most of the observed initial fast decay of SSH of Agulhas rings. Because of the growth of the $m = 2$ instability, rings deform and may eventually split. The deformation of the rings is associated with the formation of filaments and small scale structures. It has been shown in Drijfhout et al. (2003) that for the simulation of Ring Astrid the loss of passive tracer scales well with the decay of SSH, which means that the SSH decay is probably related to mixing of thermodynamic properties with its surroundings. Here, we make an effort to determine how this mixing of Agulhas ring water takes place. In this section the evolution and spreading of tracer is discussed for two different rings, one that splits and one that remains coherent.

The evolution of passive tracer in layer 1 of ring A is shown in Fig. 2. The boundary of the ring B_k, as defined in the previous section, is shown as a thick solid line. At day 20 a filament becomes visible at the eastern side of the ring, and at day 40 a second filament at the western side is seen. From this moment on the ring

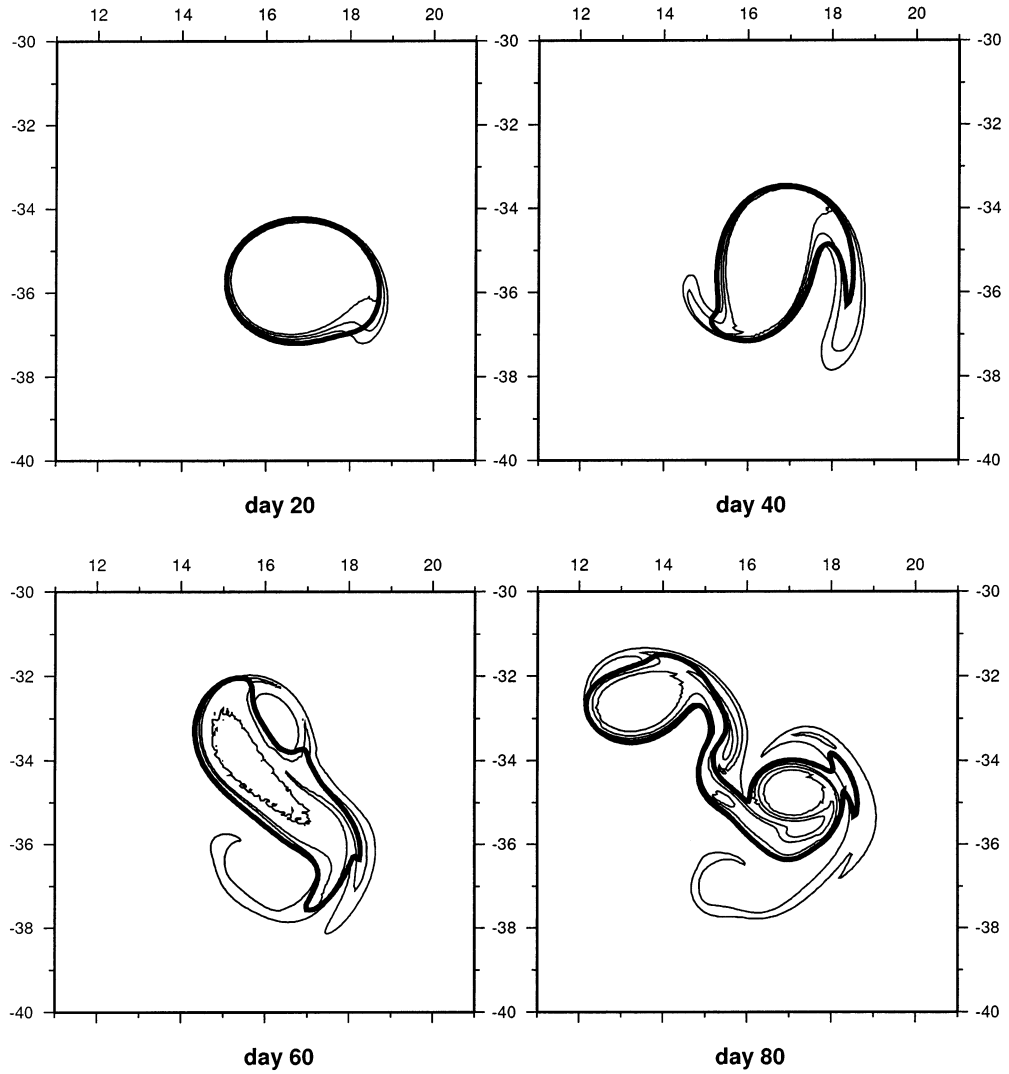

FIG. 2. Tracer concentration (contour interval = 0.3) and ring boundary B_k (thick line) for layer 1, ring A. The maximum initial value of tracer was 1.0.

deforms and elongates more and more, as is seen at day 60. Finally, at day 80 the ring has split into two halves, of which one is larger than the other. Hereafter, the two rings remain more or less stable (not shown). The tracer evolution for ring B, which remains coherent, is shown in Fig. 3. Clearly, the filaments are much smaller and thinner and the second filament is quicker formed than in the case of the larger ring, already at day 20. The ring remains coherent even though large filaments are being shed from the ring, as can be seen at day 80. During the evolution of both rings, tracer is leaking out of the ring at the extremes of the filaments. Along with leakage of water out of the rings, there is also water from outside entering the ring at the cyclonic sides of the ring filaments. This indicates that a large part of mixing of ring water takes place along the filaments. The filaments are finally separated from the ring and will be fully mixed with their surrounding water by small-scale mixing processes. Although the evolution and deformation of both rings is not the same, it seems that the process underlying the filamentation of the rings is identical. This will be investigated in the next section.

For both rings the evolution of tracer in layers 2 to 5, which corresponds to thermocline water, is qualitatively similar to the evolution in layer 1. However, the tracer leakage through the filaments is larger, whereas the lobes of the ring's pressure boundary B_k themselves are much smaller in this layer. Below the thermocline the tracer evolution behaves differently. In Fig. 4 we show the evolution of tracer in layer 10 of the largest ring A (at approximately 1600-m depth outside the ring), which is characteristic for all deep layers. Here, tracer evolution is much different from the evolution of the pressure field and does not show the two long filaments as was the case in layers 1–5. The structure of the tracer field has deformed largely as can be seen at day 60, and

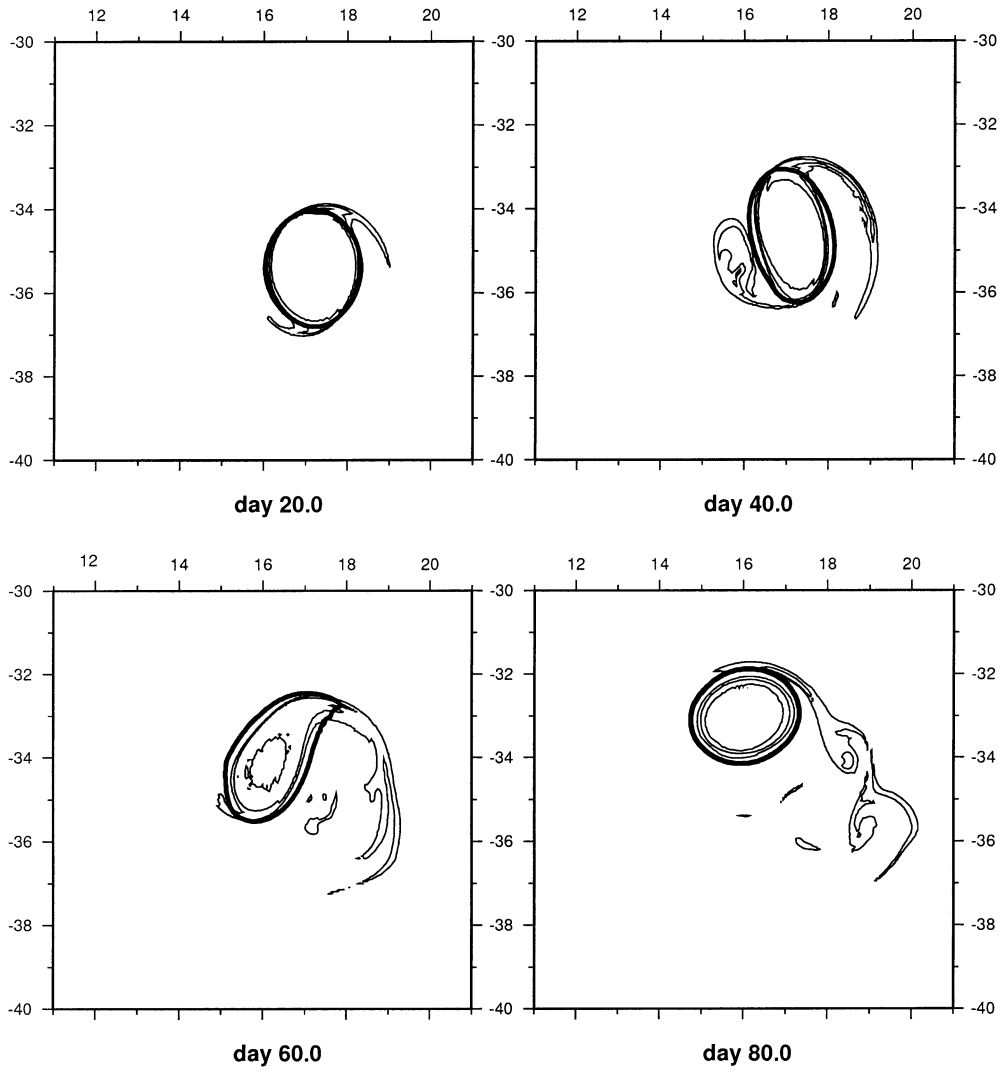

FIG. 3. Tracer concentration (contour interval = 0.3) and ring boundary B_k (thick line) for layer 1, ring B.

a large blob of tracer has evolved out of the ring. The qualitative evolution in the lower layers for ring B is identical as for ring A and is not shown here.

Describing tracer transport using a kinematic approach

In order to understand the development of the filaments and to quantify the transport of tracer from the ring, different methods can be used. In certain (geophysical) flows transport and mixing processes can be determined with methods that have their roots in dynamical systems theory. Using segments of intersecting stable and unstable manifolds associated with the hyperbolicity of the flow, lobe transport of fluid from one flow regime to another can be determined. However, these methods have not been developed well enough to determine the fluid transport for our three-dimensional flow discussed here since the time dependence of the hyperbolicity of the rings is too strong. For further details, see the appendix.

Since the method from dynamical systems theory cannot be used to derive a ring boundary, we have to turn to another, more approximate, method. Here, we will introduce a kinematic separatrix derived from a streamfunction of the nondivergent part of the flow, as an estimate of the ring boundary. This kinematic approach does not provide an exact way of quantifying the leakage due to the fact that the streamlines are not paths of water parcels, but instead only show the nondivergent part of the flow at one specific instant in time.

To use the concept of a separatrix one has to be able to define a streamfunction ψ. Of the two rings we consider here, neither is steadily propagating, and so the determination of a streamfunction is not straightforward. First we determine the streamfunction that relates to the divergence free transport, simply found by solving $\Delta\psi = \nabla \times [h_k(\mathbf{u}_k - \mathbf{u}^{\text{trans}})]$. The translation velocity

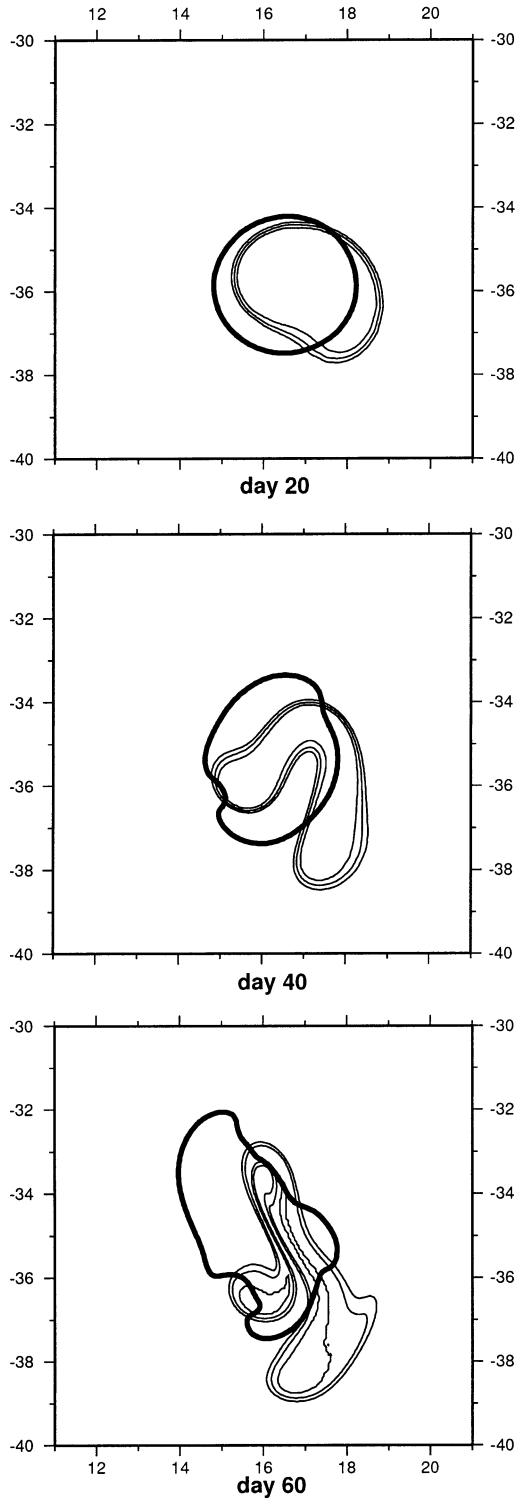

FIG. 4. Tracer concentration (contour interval = 0.3) and ring boundary B_k (thick line) for layer 10, ring A.

$\mathbf{u}_k^{\text{trans}}$ of the ring is determined at the maximum interface displacement, averaged over a 10-day period to filter out fast internal gravity waves.

To determine how this field relates to the total transport field we calculate the following two functions:

$$\psi^x = +\int_{x^0}^{x} h(v - v^{\text{trans}})\, dx + \psi^x(x^0) \qquad \text{and} \qquad (3)$$

$$\psi^y = -\int_{y^0}^{y} h(u - u^{\text{trans}})\, dy + \psi^y(y^0), \qquad (4)$$

where $\psi^x(x^0)$ is equal to $h(u - u^{\text{trans}})$ integrated meridionally at $x = x^0$, and $\psi^y(y^0)$ is equal to $h(v - v^{\text{trans}})$ integrated zonally at $y = y^0$. When the streamfunction does not deviate more than 5% of either of these two functions, it is closely related to the total transport and is used in the subsequent analysis. This procedure is followed for all layers. For ring B, the smaller coherent ring, the streamfunction is well defined during the total evolution. For ring A, the splitting ring, the definition of the streamfunction can only be used during the first 40 days because of the growing $m = 2$ instability.

The translation speed of ring A ranges from 2.5 to 5 km day^{-1}, which matches observed translation speeds of Agulhas rings (Goñi et al. 1997; Schouten et al. 2000). In Fig. 5 the streamfunction is shown on top of the tracer distribution for layer 1 at day 10, 20, 30, and 40. The separatrix shows a stagnation point, where $(u_1 - u_1^{\text{trans}}) = (v_1 - v_1^{\text{trans}}) = 0$, at the northeastern side of the ring. Within the separatrix the streamlines are closed (not shown) and outside the separatrix they are open. The water inside the separatrix has a swirl speed that is larger than the translation speed and will be transported within the ring. It is clear that the separatrix is not steady and that it changes its shape during the ring evolution.

At the southeastern side the first filament starts to develop as can be seen at day 20. The tracer filament follows more or less the shape of the separatrix at day 10 and 20. From day 30 on, a second filament is formed at the western side of the ring. The second filament remains relatively small compared to the first, fast growing filament.

The filaments in the upper five layers of ring A are larger than in layer 1, but the shape and evolution is identical. The filaments become larger with depth because of the smaller swirl velocities and thus, to a smaller separatrix. Figure 6 shows the streamfunction evolution of layer 10. The separatrix here is much smaller and decreases faster with time than in the upper layers because of changing flow properties; the ring becomes less barotropic and eventually a small dipolar structure arises in the lower layers (not shown).

Although ring B equilibrates much faster than ring A, its tracer evolution is more chaotic; see Fig. 7. Also in ring B two filaments are formed. The filament that originates at the northeastern side is developing even faster

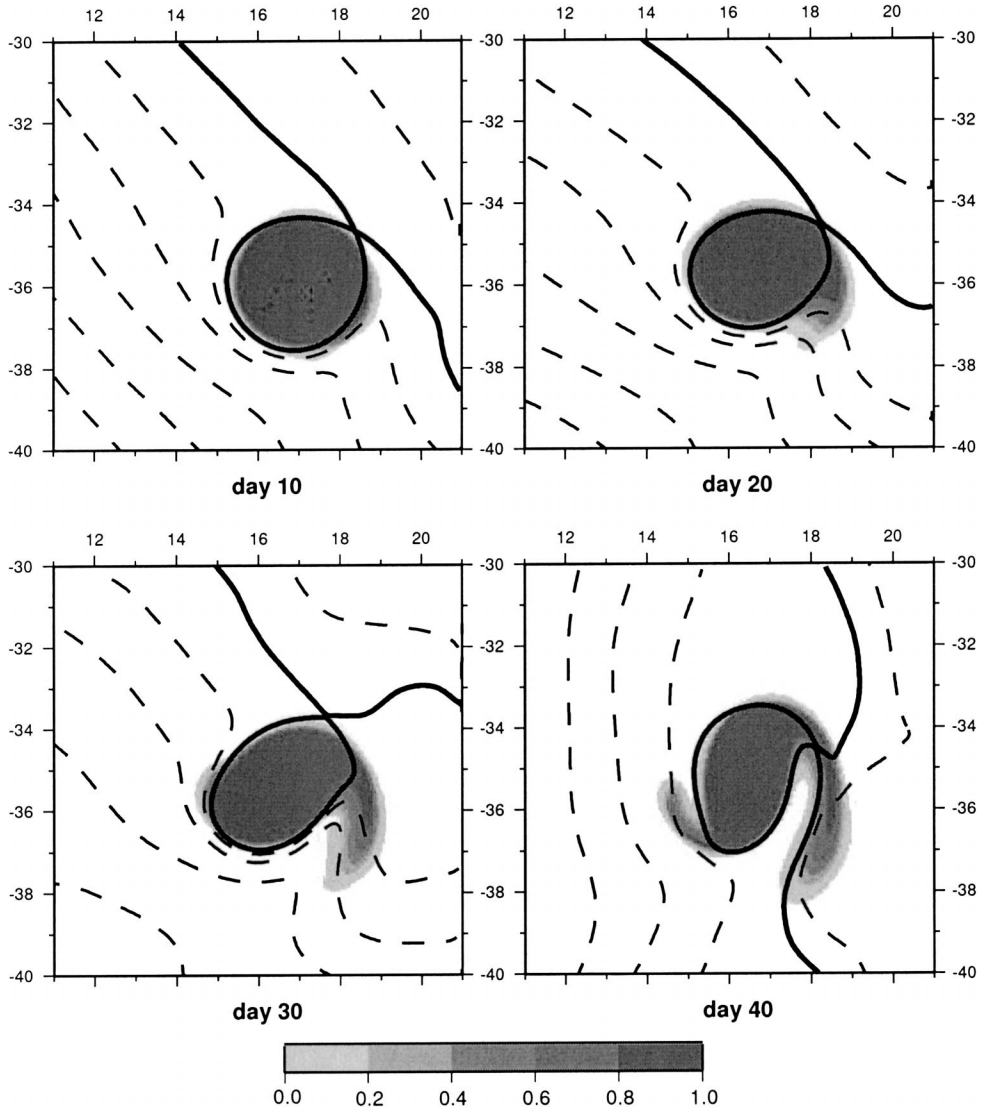

FIG. 5. Tracer concentration (contour interval = 0.2), streamlines (dashed lines), and separatrix (thick line) for layer 1, ring A.

and its growth is enhanced by the rapid motion of the stagnation point at that side (see also Fig. 12). The streamfunction evolution in the lower layers is similar to that of ring A and is not discussed further. Even though this ring remains coherent, the enhanced, asymmetric filamentation process is identical to that of ring A.

4. Quantifying tracer leakage

Even though an exact analysis of mixing of ring water is not achieved in this paper, we do try to make an estimate of the mixing by defining a ring boundary and estimating the amount of leakage of tracer over this boundary. One way of defining a boundary is to determine the separatrix in a kinematic way as was described above. This provides us only with an estimate of the flux of tracer from one moment to another moment in time. Another way of making an estimate is to determine the flux across the maximum density gradient of the ring, where the maximum swirl velocities are found. Such a boundary is usually applied when evaluating transport from in situ data (Olson and Evans 1986; De Ruijter et al. 1999 for an overview). In this section we make a comparison of the estimated leakage using three different ring boundaries: 1) the boundary B_k within which the tracer was initialized, 2) the kinematic separatrix, and 3) a boundary defined as the maximum density gradient.

First the decay of tracer content within ring A as a function of time, using B_k as the boundary, is shown in Fig. 8. Initially there is fast decay of the total tracer content within the ring, which lasts until day 50 after

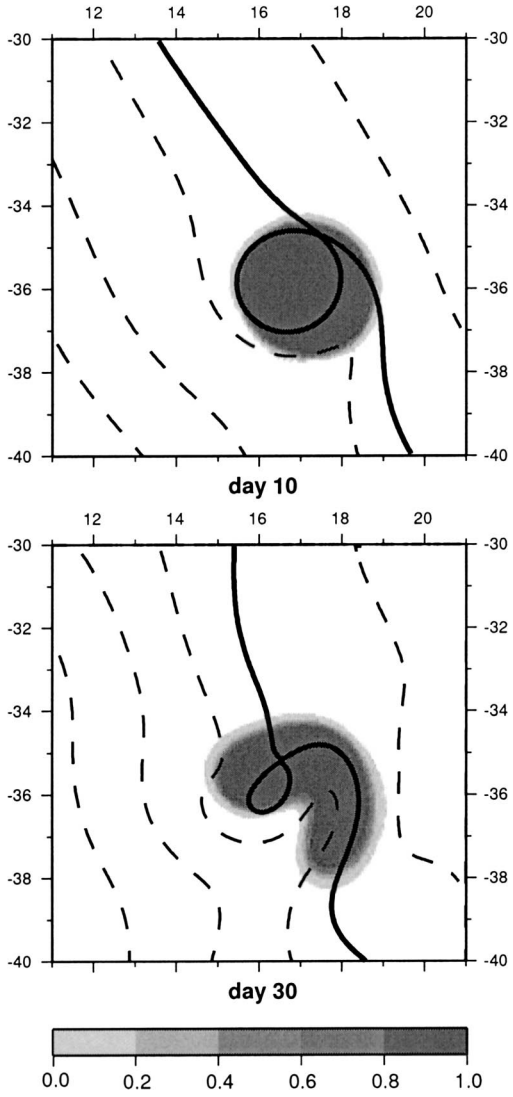

FIG. 6. Tracer concentration (contour interval = 0.2), streamlines (dashed lines), and separatrix (thick line) for layer 10, ring A.

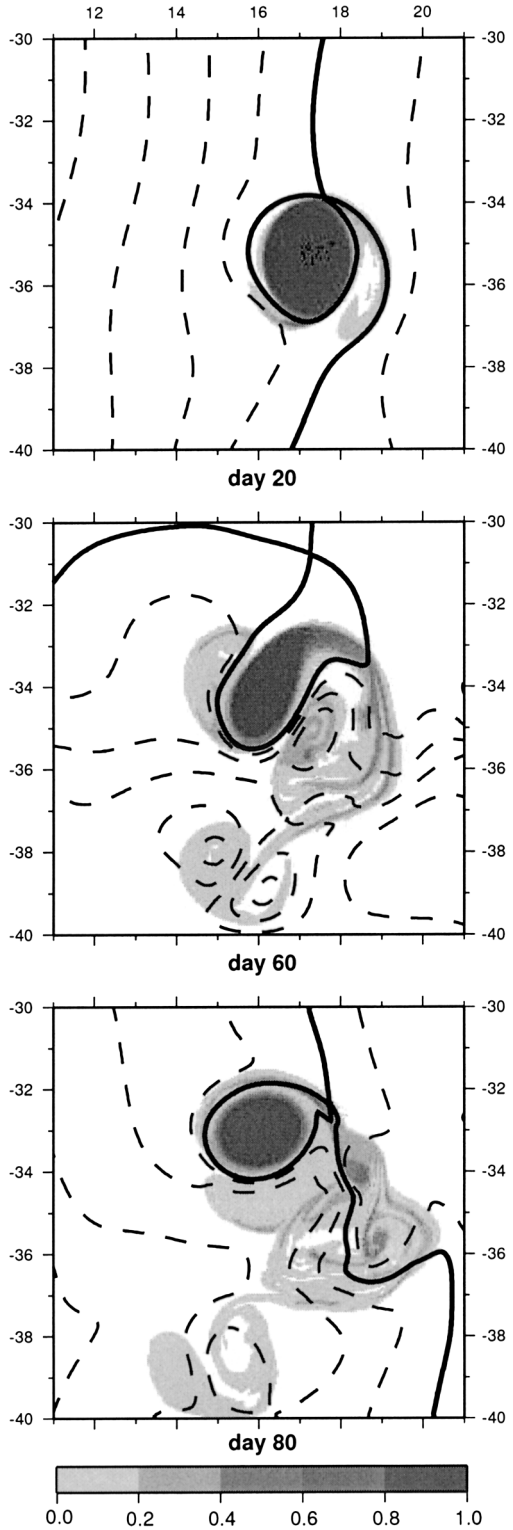

FIG. 7. Tracer concentration (contour interval = 0.2), streamlines (dashed lines), and separatrix (thick line) for layer 1, ring B.

which the decay levels off. There are large differences in tracer decay for the different layers. In layer 1 the decrease of enclosed tracer content is approximately 25% in 80 days. The decay is much larger in layer 5 and largest decay is in layer 10, where the enclosed tracer content decreases by more than 50%. The total loss of tracer in the ring is 45%. For ring B the decay of tracer is shown in Fig. 9. Overall, the decay of tracer content is larger for this ring, about 55% in total. However, qualitatively the results are the same for both rings: the decrease of tracer content is smallest in layer 1, it is largest in layer 10 and the decay rate decreases after approximately 50 days.

To determine how tracer content depends on the evolution of the separatrix, the amount of tracer enclosed by the separatrix in layer 1 is shown in Fig. 10. For ring A only the first 40 days are shown since during

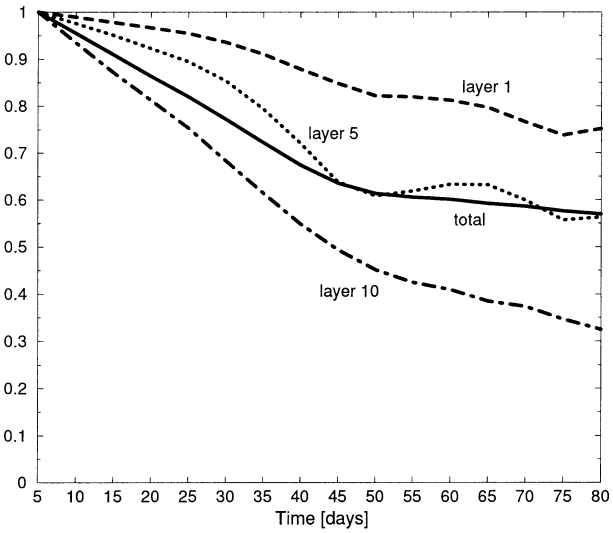

FIG. 8. Decay of tracer content within boundary B_k, ring A.

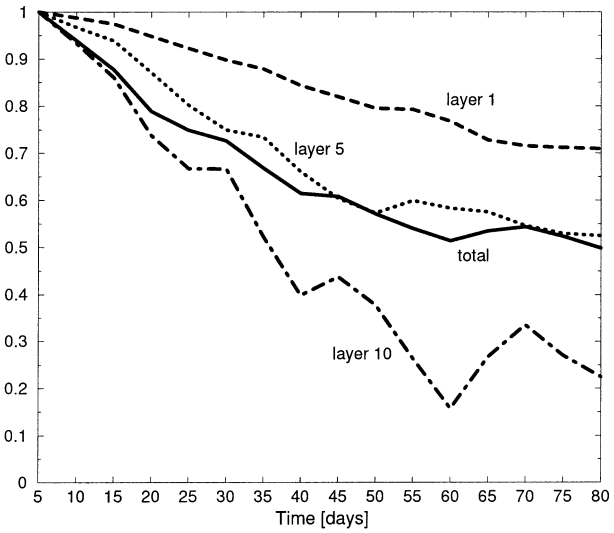

FIG. 9. Decay of tracer content within boundary B_k, ring B.

that period the streamfunction is well defined. The streamfunction for ring B is defined during the whole period of 80 days. For ring A the enclosed tracer content, using the kinematic boundary, gives qualitatively the same results as in Fig. 8. For ring B the kinematic boundary gives somewhat smaller decay in layer 1 but larger decay layer 10 (not shown) than when using B_k, however the differences are not more than 10%.

In Fig. 10 the estimated leakage for layer 1, using the maximum density gradient as a boundary, is also shown for both rings. Using this boundary the decay of tracer in ring A is larger (about 10%–15%) than when using B_k. After the splitting process of ring A the ring has become smaller and the density gradients have steepened such that the boundary of maximum density has changed. For ring B the structure of the ring has not changed much during the evolution and there is no difference in decay when using the maximum density gradient when compared with B_k. The decay for the lower layers is identical to that of the decay in Fig. 9 and is not shown here.

Even though there are small differences in the quantification of the decay, within a range of 10%–15%, the picture remains quite robust when comparing the use of three different boundaries. The total tracer content decays to about one-half for both rings, the decay is smallest in the upper layers, but it still may reach up to 35%–40%, and it is largest in layer 10, where the tracer decay is about 80%–90%.

It is quite surprising that the amount of decay of the two different rings does not differ much. Initially one would think that the splitting process would contribute largely to the decay and the mixing of ring water. Here, we have shown that the amount of tracer leakage is very insensitive to the final splitting process; the loss of tracer is even larger for the coherent ring, which moves more irregularly, than for the splitting ring.

5. Discussion and conclusions

Agulhas rings enter the South Atlantic subtropical gyre and ring trajectories differ from the main branch of the thermohaline circulation in the South Atlantic, which follows the Benguela Current and the South Equatorial Current toward the North Atlantic Ocean. To contribute to the upper branch of the thermohaline circulation, Agulhas rings have to mix their properties when they travel through the Cape Basin, crossing the pathway of the thermohaline circulation.

In this study we focus on the mixing that arises from ring deformation due to its instability and from the β-induced movement. We find that 40% of the ring water in the thermocline is mixed away during the first few months of the ring's lifetime. So, it is very well possible

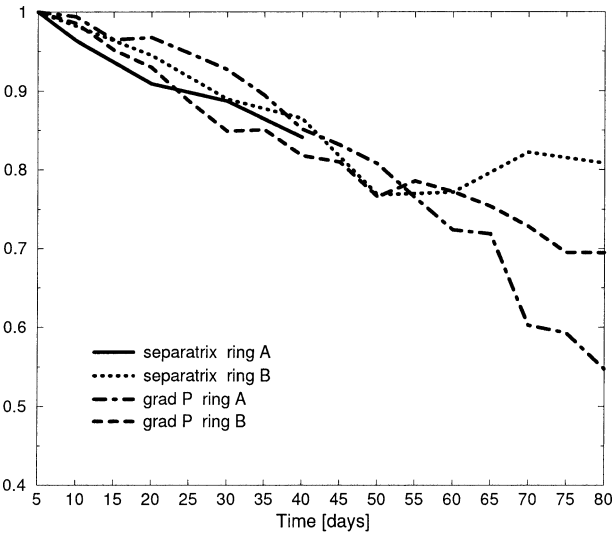

FIG. 10. Comparison of decay of tracer content using different boundaries in layer 1 for rings A and B.

that significant fractions of the heat and salt anomalies associated with Agulhas rings are entrained within the upper branch of the thermohaline circulation while the rings cross the Cape Basin. Eventually interaction with bottom topography and possibly other processes may lead to enhanced mixing of ring water with its surroundings.

The evolution of passive tracer in two different ring simulations shows that for the layers above the thermocline mixing of ring water takes place preferably at filaments, which are formed by a combination of ring deformation, differential rotation, and the β-induced movement. For deeper layers only a small part of the ring is transported with the ring. Qualitatively this can be explained well by the fact that the swirl velocities are different at each depth, which results in differences in the area enclosed by the separatrix. Most mixing takes place at that depth where the absolute swirl velocity attains a minimum value and where tracer is not held within a separatrix and can be mixed freely with the surroundings by Rossby waves. This means that, even though the ring has a significant dynamical structure at large depth, it is not necessary that thermohaline properties remain in this structure. This corresponds with measurements of Ring Astrid, during the MARE campaign, that show no distinction between thermohaline properties of ring water and surrounding water below the 12° isotherm (A. K. van Veldhoven 2003, personal communication).

For both rings the filamentation process is mainly a result of deformation of the ring due to the $m = 2$ instability and of the differential rotation of the ring. As a consequence, tracer is advected into two filaments. To determine the influence of the β effect on formation of these filaments, a ring simulation on the f plane was performed. In Fig. 11 the tracer evolution of ring A on the f plane is shown together with the ring boundary B_k, related to pressure (see section 2). In order to obtain growth of the $m = 2$ instability on the f plane, a perturbation is added to the initial ring profile. After about 30 days, the initially circular f-plane ring has become elliptic because of the growing $m = 2$ instability. Two symmetrical thin filaments are formed by differential rotation.

On the β plane, because of self-advection of the ring, a stagnation point in the flow arises, causing the filamentation to become asymmetric and more erratic. A comparison of the amount of tracer leakage between the f plane and β plane shows that, because of the β movement, enhanced leakage occurs in the top five layers. This ranges from 25% extra tracer loss for ring A to 40% extra for ring B in the top layer. Thus, the presence of a stagnation point due to the self-advection increases tracer loss in the top layers. This difference, however, becomes smaller with depth. In the lower layers the amount of tracer loss on the f plane and on the β plane is very small. However, the processes leading to filamentation are different: on the β plane it is governed by the fast-shrinking separatrix, corresponding with the β movement; on the f plane it is only the $m = 2$ instability that is important. Since the $m = 2$ mode is more barotropic than the ring itself (see Drijfhout et al.

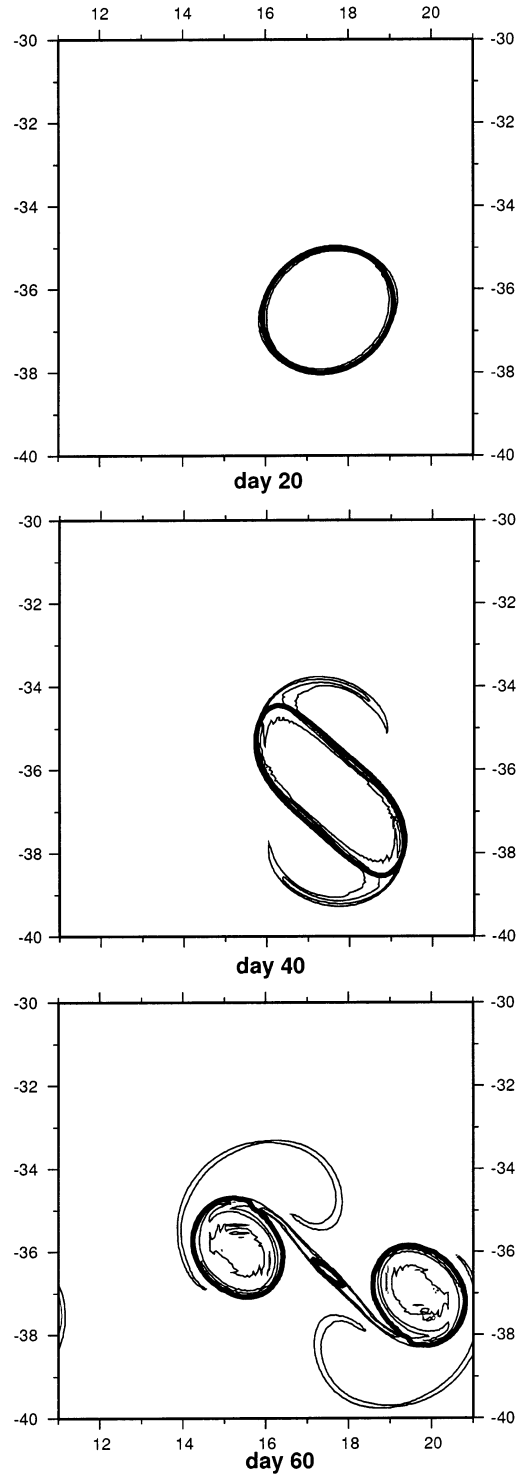

FIG. 11. Tracer concentration (contour interval = 0.3) and ring boundary B_k (thick line) for layer 1, ring A on the f plane.

2003), which means that in the lower layers the deformation because of the $m = 2$ mode is larger, the tracer leakage in the lower layers is larger than in the top layers on the f plane. The fact that on the β plane the leakage in the lower layers due to the $m = 2$ instability is not larger than on the f plane is due to the fact that, on the β plane, the energy from the $m = 2$ mode is transferred to higher order modes and the growth of the $m = 2$ mode is smaller. Thus, we would expect less leakage on the β plane because of the smaller growth of the $m = 2$ instability. On the other hand, the β-induced movement induces enhanced leakage. In the upper layers the enhancement of tracer leakage due to the β effect dominates. In the lower layers it is canceled by reduced deformation associated with the growth of the $m = 2$ mode.

Benilov (1999) has shown numerically that rings that move steadily on a β plane still experience tracer loss. This can be explained by considering a steadily moving ring that keeps its shape and has a constant westward velocity. If tracer is initialized inside a circular domain, for instance, a ring boundary defined by a pressure contour, then this domain will remain circular in a coordinate frame moving with the ring. However, if a streamfunction is defined in the moving frame, as was done in section 3a of this paper, then this streamfunction field is not circular symmetric since it has to connect to the far field velocity, which is steadily westward. This implies that tracer has to cross the streamfunction contours, and more specifically the separatrix, and tracer leakage will occur also for a steadily moving ring. The Benilov mechanism would cause tracer loss on the β plane only, while tracer loss on the f plane would be absent. For the rings we consider this is not the case. On the f-plane filamentation is mainly governed by the $m = 2$ instability and differential rotation. The asymmetric growth of the filaments and the tracer loss on the β plane are due to the Benilov mechanism and deformation due to the instability, which is enhanced by irregular ring movement. This explains why the more erratically moving, nonlinear but equilibrating, ring B suffers more tracer loss than the more steadily moving ring A in which the growing $m = 2$ instability causes the ring to split.

The traditional subgrid parameterization of mixing by eddy diffusivity in the form of downgradient mixing is inadequate when filamentation is present. More specifically, filamentation initially increases the largest temperature and salinity gradients locally, when tracer is stirred throughout the filaments. Only after the filaments are shed from the ring the effective mixing is dominated by small-scale processes erasing the gradients associated with the boundary of the ring.

Drijfhout et al. (2003) suggested that SSH decay and tracer leakage would correlate well, as was the case for the simulation of Ring Astrid. Our results suggest the similarity between the two processes is accidental since SSH decay is governed by instability and splitting and tracer leakage is governed by the ring's nonlinearity, in particular the irregularity of its self-advection.

The main conclusions of this paper are as follows: initially filaments develop as a result of deformation of the ring due to the $m = 2$ instability and differential rotation. The presence of a stagnation point in the flow that is related to the β-induced motion of the rings makes one of the filaments grow much faster than the other. The leakage of tracer from the rings and subsequent mixing in the thermocline is mainly due to the growing of these filaments while in the deeper layers the separatrix shrinks because of the fast-changing flow field, leading to fast tracer loss. In the early stage of ring evolution 40% of thermocline ring water, carrying the largest heat and salt anomalies, is mixed away and can be entrained within the upper branch of the thermohaline circulation.

Acknowledgments. We thank Will de Ruijter for stimulating discussions and Bill Dewar for providing some helpful suggestions. We also thank two anonymous reviewers for their critiques, and Steve Wiggins for giving us more insight into chaotic transport. This research is part of the MARE project and the CLIVARNET program and was funded by the Foundation for Earth and Live Sciences (ALW) of the Netherlands Foundation of Scientific Research (NWO) under Grant 750-712.00B.

APPENDIX

Stable and Unstable Manifolds

In certain (geophysical) flows transport and mixing processes can be determined with methods that have their roots in dynamical systems theory. Two-dimensional, incompressible velocity fields form a Hamiltonian system and, if the flow is time periodic, then the study of the flow field can be reduced to the study of a two-dimensional Poincaré map (Rom-Kedar and Wiggins 1990; Wiggins 1992). For these flows, chaotic transport or mixing of particles can be analyzed in terms of the geometry of intersecting stable and unstable manifolds associated with the hyperbolicity of the flow. The lobes that result from the intersecting manifolds determine the transport of fluid from one flow regime to another. This theory has been extended to flows that have a more general time dependence: flows that have a time dependence close to being periodic (Duan and Wiggins 1996; Miller et al. 1997; Malhotra and Wiggins 1998; Rogerson et al. 1999) and flows that have a slowly varying time dependence (Haller and Poje 1998; Poje and Haller 1999).

In Miller et al. (1997) a numerical method has been developed for approximating invariant manifolds of hyperbolic fixed points in an quasiperiodic vector field. A necessary condition for determining the manifolds is that the velocity field has a strong hyperbolicity on time scales longer than the dominant time period of the flow.

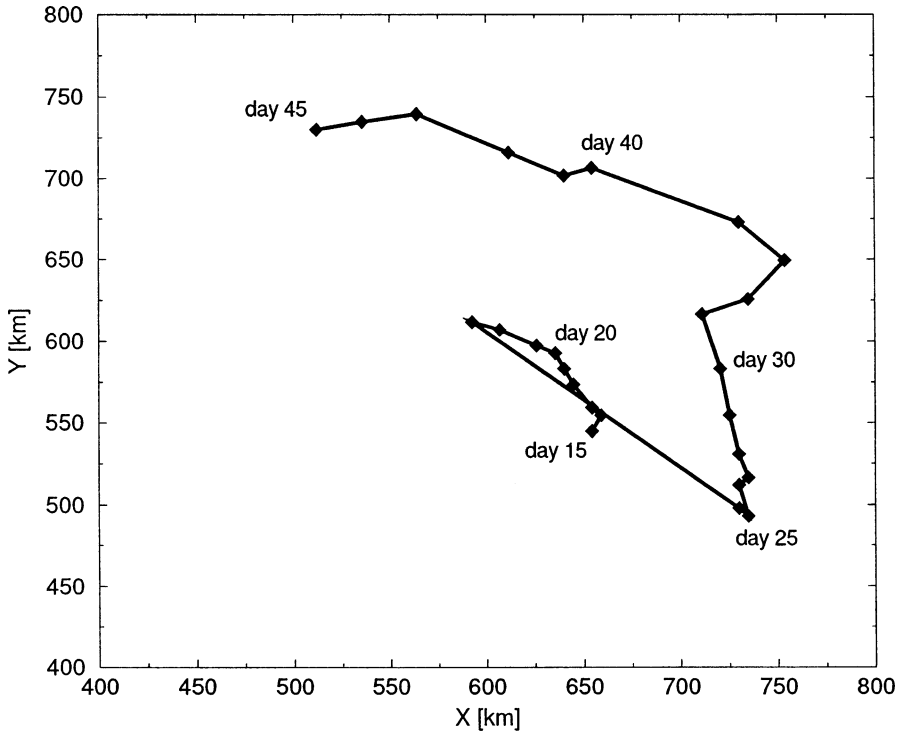

FIG. A1. Location of the stagnation point in *x–y* space during the time interval 15–45 days.

To obtain the unstable manifold, particles on a segment close to the saddle point and aligned in the direction of the unstable eigenvector are traced forward in time. The stable manifold is determined by tracing particles backward in time, which were initially aligned along the direction of the stable eigenvector. Even though this method of lobe analysis gives good results for almost periodic flows, it is not straightforward to extend the method for flows whose hyperbolicity is of transient nature.

Haller and Poje (1998) derived conditions to determine whether the time dependence of the hyperbolic point is weak enough to assume a certain hyperbolicity within a finite time interval. These conditions basically require that the speed of the stagnation point should be below a critical value, which defines a time scale over which the Eulerian and Lagrangian dynamics become uncorrelated. This time scale has to be larger than the time scale that characterizes the flow. In Miller et al. (2002) the method of lobe analysis has been applied to a time dependent recirculation and the Lagrangian boundary provided a good way to determine and quantify chaotic transport within a certain time interval. Time dependence was introduced here by increasing the wind forcing. Lobe transport could be visualized and quantified only within a time period where the hyperbolic point and the lobe transports did not show large time dependence.

Here, we started to determine finite-time manifolds for ring B using the technique described in Miller et al. (1997, 2002). Ring B remains coherent and its time dependence is weaker than for ring A, thus we expect that the method of lobe analysis can be applied. First, the saddle-type stagnation point is determined in the frozen-time Eulerian vector field in the frame of the moving ring, which is determined at the maximum interface displacement, averaged over a 10-day period to filter out fast internal gravity waves. From day 15 on, a saddle point that shows stretching and compression is found, a line segment of particles is initialized in the direction of the unstable eigenvector of the deformation matrix, and the particles are evolved forward in time using a fourth-order Runge–Kutta scheme. To obtain an approximate finite-time manifold it is necessary to insert new particles close to the saddle point at later times during the evolution. Here a problem arises since the saddle point has an erratic time dependence (see Fig. A1). As a result, it is very difficult to follow and to insert new particles during the iteration. Besides that, because of the fact that the flow is, in fact, three-dimensional, it is not clear how well the stable and unstable manifolds can be derived from the deformation matrix of the horizontal flow field. The same problem is encountered when initializing particles close to the stagnation point at a later time interval and evolving them backward in time in the direction of the stable eigenvector. The result is that finite-time stable and unstable manifolds that are long enough to serve as a Lagrangian boundary cannot be determined using this method.

To corroborate this result we evaluated the conditions of Haller and Poje (1998) to investigate whether an approximate finite-time hyperbolic trajectory can be found for the ring. The speed of the stagnation point is determined within the time interval of 15–100 days, and it is found that the maximum speed may reach up to 20 km day^{-1} for ring B and 10 km day^{-1} for ring A. The criterion of Haller and Poje (which is a function of the eigenvalues and eigenvectors of the deformation matrix, its time derivatives, and the strength of nonlinear terms close to the hyperbolic point) requires a speed of less than 1 km day^{-1}. Thus, meaningful approximations of the finite-time stable and unstable manifolds that can be used as a Lagrangian boundary are not found. Although the attempts here to determine manifolds for the ring have failed, it does not mean that there are no stable and unstable manifolds present in the flow. Recently, new analytic and numerical methods have been developed to determine Langrangian structures in vector fields with arbitrary time dependence (Ide et al. 2002; Mancho et al. 2003). So far, these techniques have been applied to two-dimensional flows only. Although the techniques do not guarantee that stable and unstable manifolds can be found for the flow fields used here, it is worthwhile to apply them to these flow fields as soon as the techniques have been extended and tested for three-dimensional velocity fields (S. Wiggins 2003, personal communication).

REFERENCES

Benilov, E. S., 1999: On the advection of tracer by eddies on the beta-plane: A numerical study. *Nonlinear Processes Geophys.,* **6,** 67–77.

Bleck, R., and L. T. Smith, 1990: A wind-driven isopycnic coordinate model of the north and equatorial Atlantic Ocean. Part 1: Model development and supporting experiments. *J. Geophys. Res.,* **95,** 3273–3505.

Byrne, D. A., A. L. Gordon, and W. F. Haxby, 1995: Agulhas eddies: A synoptic view using Geosat ERM data. *J. Phys. Oceanogr.,* **25,** 902–917.

Carnevale, G. F., and R. C. Kloosterziel, 1994: Lobe shedding from propagating vortices. *Physica D,* **76,** 147–167.

De Ruijter, W. P. M., A. Biastoch, S. S. Drijfhout, J. R. E. Lutjeharms, R. P. Matano, T. Pichevin, P. J. Van Leeuwen, and W. Weijer, 1999: Indian–Atlantic interocean exchange: Dynamics, estimation and impact. *J. Geophys. Res.,* **104,** 20 888–20 910.

Dewar, W. K., and G. R. Flierl, 1985: Particle trajectories and simple models of transport in coherent vortices. *Dyn. Atmos. Oceans,* **9,** 215–252.

Drijfhout, S. S., C. A. Katsman, L. De Steur, P. C. F. Van der Vaart, P. J. Van Leeuwen, and C. Veth, 2003: Modeling the initial fast, sea surface height decay of Agulhas ring ''Astrid.'' *Deep-Sea Res.,* **50,** 299–319.

Duan, J., and S. Wiggins, 1996: Fluid exchange across a meandering jet with quasiperiodic variability. *J. Phys. Oceanogr.,* **26,** 1176–1188.

Duncombe Rae, C. M., S. L. Garzoli, and A. L. Gordon, 1996: The eddy field of the southeast Atlantic Ocean: A statistical census from the Benguela Sources and Transports project. *J. Geophys. Res.,* **101,** 11 949–11 964.

Feron, R. C. V., W. P. M. De Ruijter, and D. Oskam, 1992: Ring-shedding in the Agulhas Current system. *J. Geophys. Res.,* **97,** 9467–9477.

Flór, J. B., and G. J. F. van Heijst, 1996: Stable and unstable monopolar vortices in a stratified fluid. *J. Fluid Mech.,* **311,** 257–287.

Goñi, G. J., S. L. Garzoli, A. J. Roubicek, D. B. Olson, and O. B. Brown, 1997: Agulhas ring dynamics from TOPEX/Poseidon satellite altimeter data. *J. Mar. Res.,* **56,** 861–883.

Gordon, A. L., 1986: Interocean exchange of thermocline water. *J. Geophys. Res.,* **91,** 5037–5046.

Haller, G., and A. C. Poje, 1998: Finite time transport in aperiodic flows. *Physica D,* **119,** 352–380.

Ide, K., D. Small, and S. Wiggins, 2002: Distuinguished hyperbolic trajectories in time dependent fluid flows: Analytical and computational approach for velocity fields defined as data sets. *Nonlinear Processes Geophys.,* **9,** 237–263.

Joyce, T. M., J. K. B. Bishop, and O. B. Brown, 1992: Observations of offshore shelf-water transport induced by a warm-core ring. *Deep-Sea Res.,* **39** (Suppl.), S97–S113.

Katsman, C. A., P. C. F. Van der Vaart, H. A. Dijkstra, and W. P. M. De Ruijter, 2003: Stability of multilayer ocean vortices: A parameter study including realistic Gulf Stream and Agulhas rings. *J. Phys. Oceanogr.,* **33,** 1197–1218.

Kloosterziel, R. C., and G. J. F. Van Heijst, 1992: The evolution of stable barotropic vortices in a rotation free-surface fluid. *J. Fluid Mech.,* **239,** 607–629.

Legras, B., and D. G. Dritschel, 1993: Vortex stripping and the generation of high vorticity gradients in two-dimensional flows. *Appl. Sci. Res.,* **51,** 445–455.

Lutjeharms, J. R. E., and J. Cooper, 1996: Interbasin leakage through Agulhas current filaments. *Deep-Sea Res.,* **43,** 213–238.

Malhotra, N., and S. Wiggins, 1998: Geometric structures, lobe dynamics, and Lagrangian transport in flows with aperiodic time dependence, with applications to Rossby wave flow. *J. Nonlinear Sci.,* **8,** 401–456.

Mancho, A. M., D. Small, S. Wiggins, and K. Ide, 2003: Computation of stable and unstable manifolds of hyperbolic trajectories in two-dimensional, aperiodically time dependent vector fields. *Physica D,* **182,** 188–222.

Miller, P. D., C. K. R. T. Jones, A. M. Rogerson, and L. J. Pratt, 1997: Quantifying transport in numerically generated velocity fields. *Physica D,* **110,** 105–122.

——, L. J. Pratt, K. R. Helfrich, and C. K. R. T. Jones, 2002: Chaotic transport of mass and potential vorticity for an island recirculation. *J. Phys. Oceanogr.,* **32,** 80–102.

Olson, D. B., and R. H. Evans, 1986: Rings in the Agulhas Current. *Deep-Sea Res.,* **33,** 27–42.

Pierrehumbert, R. T., 1991: Chaotic mixing of tracer and vorticity by modulated traveling Rossby waves. *Geophys. Astrophys. Fluid Dyn.,* **58,** 285–319.

Poje, A. C., and G. Haller, 1999: Geometry of cross-stream mixing in a double-gyre ocean model. *J. Phys. Oceanogr.,* **29,** 1649–1665.

Rogerson, A. M., P. D. Miller, L. J. Pratt, and C. K. R. T. Jones, 1999: Lagrangian motion and fluid exchange in a barotropic meandering jet. *J. Phys. Oceanogr.,* **29,** 2635–2655.

Rom-Kedar, V., and S. Wiggins, 1990: Transport in two-dimensional maps. *Arch. Rat. Mech. Anal.,* **214,** 239–298.

Schouten, M. W., W. P. M. De Ruijter, and P. J. Van Leeuwen, 2000: Translation, decay and splitting of Agulhas rings in the southeastern Atlantic Ocean. *J. Geophys. Res.,* **105,** 21 913–21 925.

Van Aken, H. M., A. K. Van Veldhoven, C. Veth, W. P. M. De Ruijter, P. J. Van Leeuwen, S. S. Drijfhout, C. P. Whittle, and M. Rouault, 2003: Observations of a young Agulhas ring, Astrid, during MARE, the Mixing of Agulhas Rings Experiment. *Deep-Sea Res.,* **50,** 167–195.

Weijer, W., W. P. M. De Ruijter, H. A. Dijkstra, and P. J. Van Leeuwen, 1999: Impact of interbasin exchange on the Atlantic Overturning Circulation. *J. Phys. Oceanogr.,* **29,** 2266–2284.

Wiggins, S., 1992: *Chaotic Transport in Dynamical Systems.* Vol. 2, *Interdisciplinary Applied Mathematics*. Springer-Verlag, 301 pp.